8

Energy

8.1 The Global Energy Markets

The energy market is the largest market in the world after currencies. The two most significant drivers of energy demand are population and income growth. Since the start of the twentieth century, the world's population has more than quadrupled, with real income and primary energy consumption growing by factors of 25 and 22.5, respectively. Over the twentieth century, the global annual average 3% GDP growth rate was sustained by an annual 2% growth rate in the energy supply, while energy consumption increased from an annual equivalent of 4 barrels (23.2 MM Btu) to 13 barrels (75.4 MM Btu) of oil per person.

Figure 8.1 illustrates the global total, urban and rural population trends from 1950 to 2050. Over the last 60 years, the world has seen a rapid urbanization, with more people living in urban areas today than in rural areas. In 2007, the world's urban population exceeded the rural population historically for the first time, with 55% of the global population living in urban areas as at 2018. The percentage of people living in urban areas ranked by regions in 2018 was North America (82%), Latin America and the Caribbean (81%), Europe (74%) and Oceania (68%). In Asia, the level of urbanization has reached approximately 50% of the population, while Africa continues to have a rural majority, with 43% living in urban areas.

The growth in urban populations is being driven by the expansion in the general population and people increasingly living in urban areas. These two factors are estimated to add an additional 2.5 billion to the world's urban

J. Rogers, *Strategy, Value and Risk*, Global Financial Markets,
https://doi.org/10.1007/978-3-030-21978-9_8

population, with the total global population estimated to reach 9.7 billion by mid-century.

Urban population growth is therefore expected to continue, with close to two-thirds of the global population living in urban areas by 2050. Urbanization levels will, however, vary significantly across regions. Close to 90% of the urban growth is expected to occur in Asia and Africa, with urbanization by the mid-century reaching 64% and 56%, respectively.

Figure 8.2 illustrates the long-term real GDP forecasts by region from 2020 to 2050. Global total long-term real GDP is forecast to rise from $103 trillion

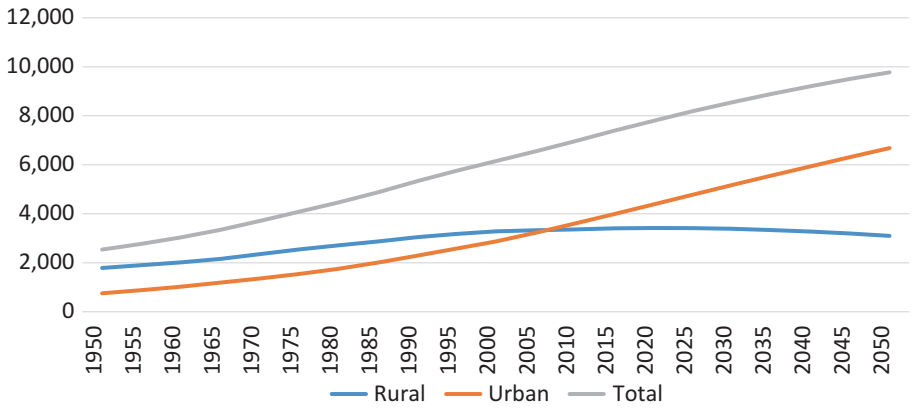

Fig. 8.1 Rural, urban and total population trends, 1950–2050 (M). Source: United Nations, Department of Economic and Social Affairs, Population Division (2018). World Urbanization Prospects: The 2018 Revision, Online Edition

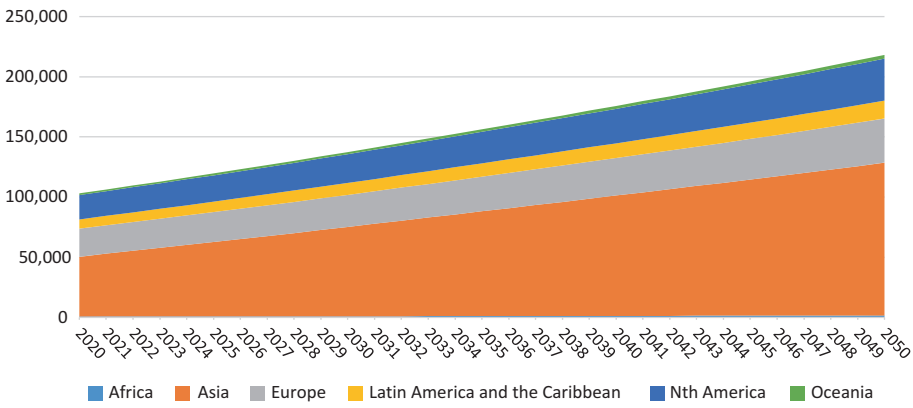

Fig. 8.2 Real long-term GDP forecast by region (billions US dollars). Source: data.oecd.org (2018), GDP long-term forecast (indicator) measured in US dollars at 2010 purchasing power parities, https://data.oecd.org/gdp/gdp-long-term-forecast.htm

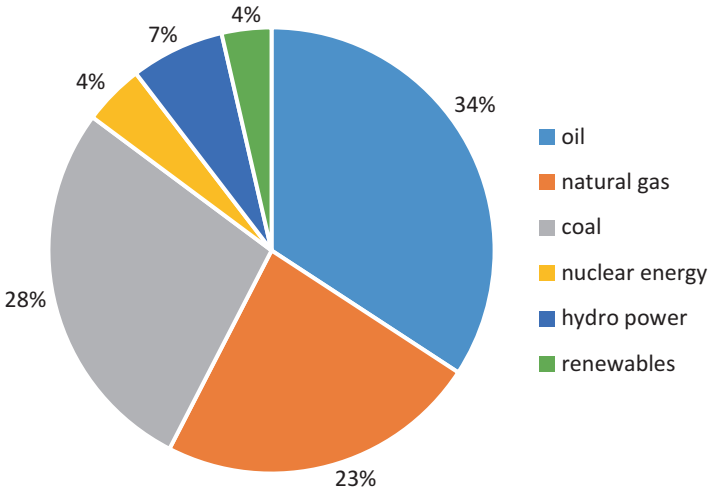

Fig. 8.3 Total world primary energy consumption by fuel. (13,511.2 million total tonnes of oil equivalent). Source: BP Statistical Review of World Energy, June 2018

to $218 trillion; in Europe, from $23.4 to $36.6 trillion; and in North America, from $20.3 to $34.9 trillion. The real GDP forecast for Asia is $49.7 to $126.9 trillion, with China ($24.9 to $54.4 trillion, a 118% increase) and India ($10.1 to $41.5 trillion, a 311% increase) a significant component of Asian growth. Real GDP growth in Latin America and the Caribbean is projected to rise from $7.6 to $15.0 trillion; in Africa, from $740 billion to $1.7 trillion; and in Oceania, from $1.4 to $3.1 trillion.

Figure 8.3 illustrates the total world primary energy consumption by fuel as at 2017, with nuclear 4%, renewables 4%, hydro power 7%, natural gas (NG) 23%, coal 28% and oil 34%.

Figure 8.4 shows the forecast for the world energy consumption by fuel from 2020 to 2040. The forecast for petroleum and other liquids (including biofuels) is 202.2 to 229.5 quadrillion British Thermal Units (quad Btu), a 13.5% increase; natural gas, from 132.2 to 181.6 quad Btu, a 37.4% increase; coal, from 162.3 to 160.9 quad Btu, a 0.9% decrease; nuclear, from 28.5 to 37.9 quad Btu, a 33% increase; and renewable energy (excluding biofuels), from 84.7 to 128.8 quad Btu, a 52% increase.

Figure 8.5 shows the forecast for global energy consumption by region from 2020 to 2040. By 2016, the world was consuming a total of 572.8 quad Btu of energy per year, and is forecast to rise to 736 quad Btu in 2040. Non-OECD (Organisation for Economic Co-operation and Development) regions are expected to account for most of the global growth in energy consumption,

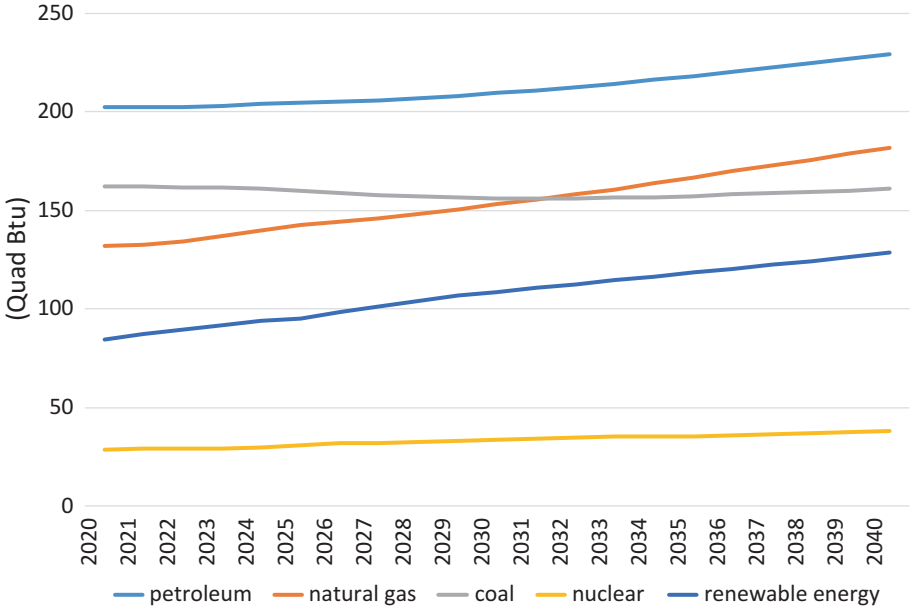

Fig. 8.4 World energy consumption by energy source, 2020–2040 (Quad Btu). Source: U.S. Energy Information Administration, International Energy Outlook (2017). Note: Petroleum and other liquids includes biofuels; renewable energy excludes biofuels

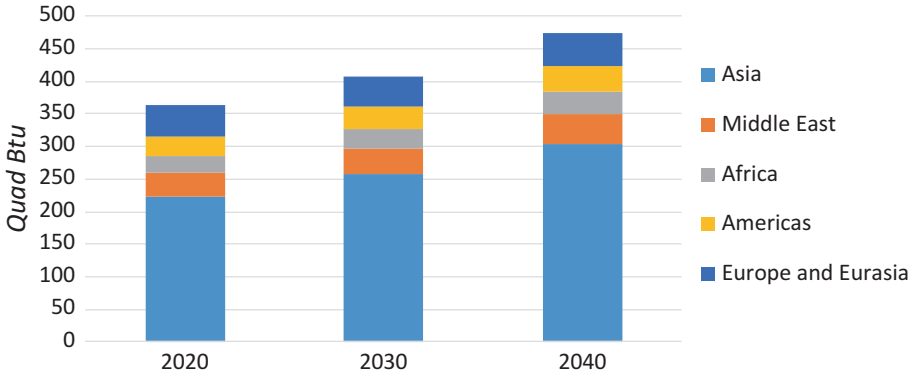

Fig. 8.5 Non-OECD energy consumption by region, 2020–2040 (Quad Btu). Source: IEA Annual Energy Outlook 2018

with increasing energy demand driven by long-term economic growth. Greater than 50% of the global increase in energy consumption will occur in Asia, predominantly in China and India, and by 2040, will exceed OECD energy use by 41 quad Btu.

Efficiency improvements are also likely to be a factor in energy demand. Energy efficiency—generally defined as the energy to GDP ratio or energy per unit of GDP—is forecast to accelerate and factor into income growth over the next 20 years, with more rapid efficiency gains seen in non-OECD economies.

8.2 The Transformation of the Energy Sector

The global energy sector is currently undergoing a fundamental transformation. Driving this process are the growth and cost competiveness of fossil fuel alternatives that include renewables, the rise of electric vehicles, the globalization of natural gas markets, gains in energy efficiency, battery developments and greenhouse gas emission issues.

These trends are creating unparalleled pressure within the oil industry. As the global energy market more than doubled in size since 1971, fossil fuels remained relatively stable in the energy mix at 80–85% of the total energy market. In 2016, however, the beginnings of a structural change emerged in the energy markets, with the global share of electricity produced by wind and solar rising from 4.5% to 5.2% (International Energy Agency [IEA] figures).

The future global demand for oil is a fundamental component of this structural change. The peak demand for oil is predicted to arrive as early as 2025 and any time up to the late 2040s. This peak will not be the result of the typical oil price cycle, and instead, signify a structural change in energy consumption, in which oil prices begin a slow permanent decline to a level where oil investments are uneconomic.

The International Energy Agency's (IEA) New Policies Scenario (NPS) includes current and planned policies that will have an impact on future energy demand and supply, distribution, carbon emissions, air pollution and all fuels and technologies within the energy system in general. Figure 8.6 shows the oil demand in mb/d under the NPS from 2025 to 2040. The growth in energy demand in the NPS is forecast to be more than 25% to 2040, and require greater than $2 trillion in new energy supply investment per annum. Renewables will constitute more than 60% of gross additional capacity to 2040, and reach 50% of global power generation capacity in most regions by 2035.

One of the fastest growing energy technologies in the NPS is solar photovoltaic (PV), which is forecast to have the second largest installed capacity behind hydro generation, surpassing wind capacity in the near future and coal before 2040. China and India will be the main drivers of the growth in global solar PV, with greater than 50% in additional global solar PV capacity.

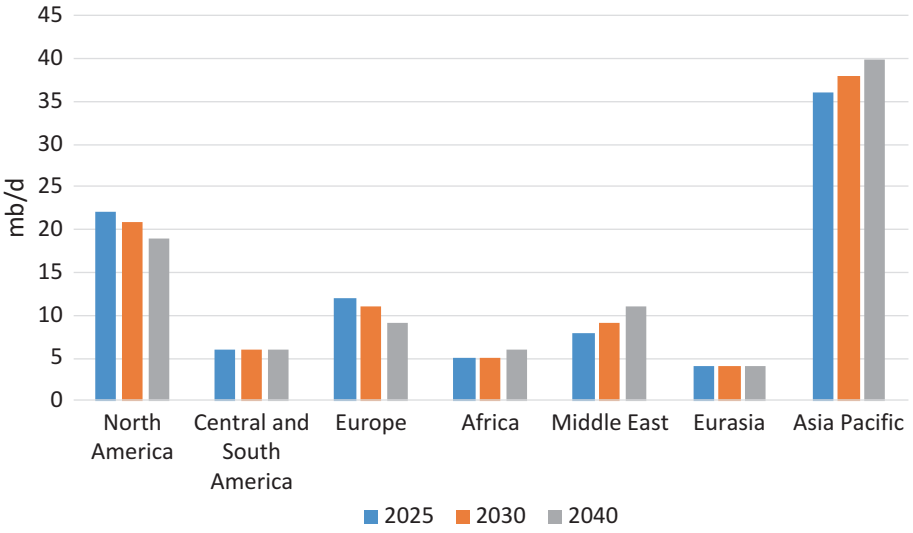

Fig. 8.6 Oil demand under the IEA New Policies Scenario, 2025–2040 (mb/d). Source: IEA World Energy Outlook 2018

Installed wind power will also see rapid growth, reaching approximately 1700 GW or 14% of global capacity by 2040.

While global oil demand growth does slow in the NPS, peak oil does not occur before 2040, and there is no peak in global energy-related CO2 emissions. The NPS oil demand from 2025 to 2040 for North America is 22 to 19 mb/d; Central and South America, flat at 6 mb/d; Eurasia, flat at 4 mb/d; Europe, from 12 to 9 mb/d; Africa, 5 to 6 mb/d; the Middle East, 8 to 11 mb/d; and the Asia Pacific, from 36 to 40 mb/d. China under the NPS is predicted to be the globe's single largest oil consumer and net oil importer by the 2030s, importing more than 13 mb/d by 2040.

The IEA Sustainable Development Scenario (SDS) provides a sustainable energy benchmark, compared to the NPS current and planned policies, which combines three critical policy goals—climate issues, air quality and energy access. Figure 8.7 illustrates the oil demand in mb/d under the SDS from 2025 to 2040. The SDS oil demand forecasts from 2025 to 2040 are declines in North America, from 20 to 12 mb/d; Central and South America, from 5 to 4 mb/d; Europe, from 11 to 5 mb/d; the Middle East, from 8 to 7 mb/d; Eurasia, from 4 to 3 mb/d; the Asia Pacific, from 33 to 27 mb/d; and Africa, flat at 5 mb/d.

Scenarios for the future energy mix will be a function of future global energy demand and the diffusion of new energy technologies. High energy demand and low technology diffusion will see global oil demand peak around the late 2040s, with oil, and natural gas and coal approximately 25% and

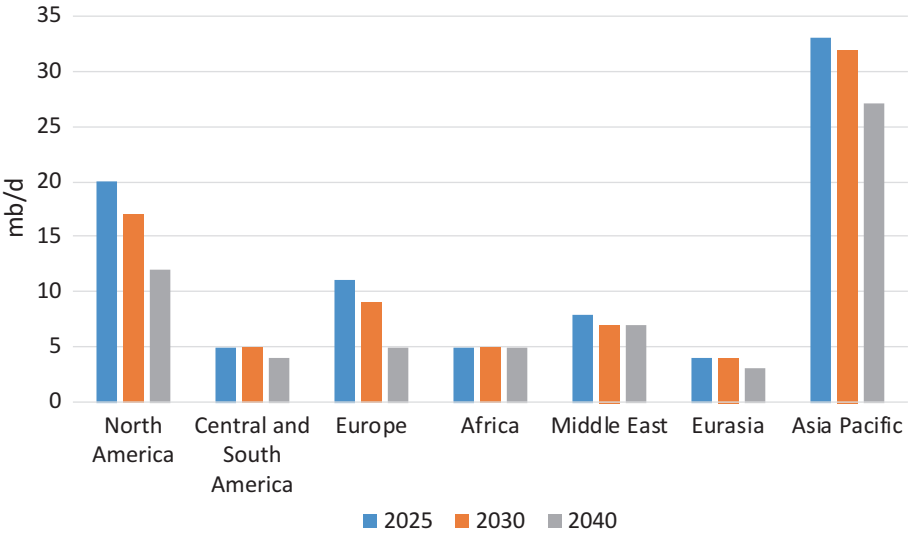

Fig. 8.7 Oil demand under the IEA Sustainable Development Scenario, 2025–2040 (mb/d). Source: IEA World Energy Outlook 2018

wind and solar 5% of total demand. Low energy demand driven by energy efficiency and high technology diffusion will potentially see global demand for oil peak as early as 2025. Under this scenario growth in global energy, demand will be significantly less by 2040, with oil and natural gas each making up approximately 25%; coal 20%; and solar and wind, 15% of total demand.

Over the twenty-first century, the trends in the energy mix will potentially see renewables reach one-half to two-thirds of the energy system, with the majority being solar energy, and wind energy in niche regional markets. Global demand for natural gas is expected to continue rising, and is viewed as a bridge fuel in the transition from fossil fuels to renewable energy. The peak natural gas forecast, however, is a function of the trends in the rapidly falling costs and continued investments in renewable energy.

These scenarios will dramatically alter energy business models, as the growth in alternative energy technologies and their declining costs transform industries across the global economy. Energy firms will therefore require the resources and capabilities to adapt to the evolving energy markets and maximize value at every stage of the energy value chain. Firms will need to decarbonize their portfolios as the energy system transforms from oil and gas to electricity and global clean energy. Those firms with capitalized oil and gas reserve exploration costs also face the risk of being unable to monetize the asset values, as downstream sales demand softens due to the structural decline in peak oil prices, and therefore, need to reduce their exposures to stranded assets.

Investment in renewable energy will therefore significantly increase in the future, as will the capabilities required to produce, sell and trade energy. Building and managing a new energy complex will require management technologies that include portfolio trading and risk management, data and analytics, and advanced methods for the analysis of energy asset investments, divestments and value.

8.3 Natural Gas and Renewables

One consequence of the long life of energy assets is that change in the energy mix is slow; however, gas and non-fossil fuels are expected to increase their share at the expense of oil and coal. The fastest growing energy source is renewable energy, with 40% of the increase in primary energy, and natural gas demand expected to see continued growth globally. By 2040, the energy mix is expected to be the most diversified in the history of the industry, as the growth of other new energy technologies develops.

Figure 8.8 illustrates the natural gas (NG) demand under the IEA Sustainable Development Scenario (SDS) in billion cubic metres (bcm) from 2020 to 2040. The globalization and growth in natural gas, supported by the US shale revolution and growth in liquefied natural gas (LNG), will continue

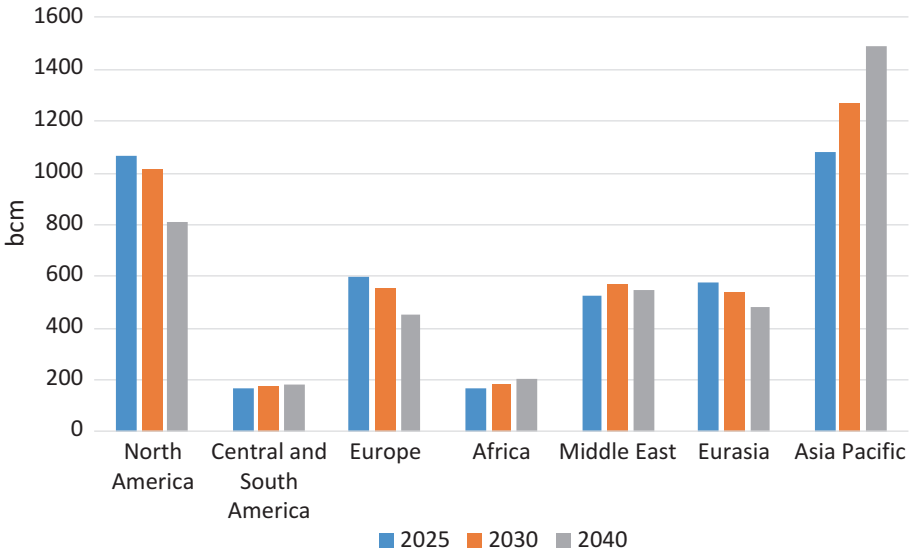

Fig. 8.8 NG demand under the IEA Sustainable Development Scenario, 2025–2040 (bcm). Source: IEA World Energy Outlook 2018

to transform the global gas markets. Gas is more responsive to short-term supply and demand dynamics, and has greater availability in markets across regions as a result. A key driver of natural gas demand growth in the Asian emerging economies are policies aimed at addressing air pollution.

NG demand under the SDS from 2025 to 2040 in North America is a decline from 1066 to 814 bcm; growth in Central and South America from 170 to 184 bcm; in Europe, a decline from 596 to 450 bcm; growth in Africa from 166 to 201 bcm; the Middle East, from 528 to 545 bcm; and in the Asia Pacific, from 1081 to 1491 bcm; and a decline in Eurasia from 574 to 485 bcm.

Figure 8.9 shows the renewables demand under the SDS from 2025 to 2040. Renewables demand under the SDS sustainable policies in terawatt hours (TWh) in North America is 1841 to 3719 TWh; Central and South America, 1155 to 1773 TWh; Europe, 1569 to 2537 TWh; Africa, 410 to 1528 TWh; the Middle East, 125 to 956 TWh; Eurasia, from 321 to 725 TWh; and Asia Pacific, 5013 to 12,481 TWh.

Wind energy is a renewable energy technology that uses the physics of wind to drive turbines that generate electricity, and is one of the fastest growing energy technologies in the world today.

Wind turbines are combined into wind farms that provide scale, and can either be connected to electricity transmission grids and networks for distribution or provide electricity to meet off-grid demand. The advantages of wind

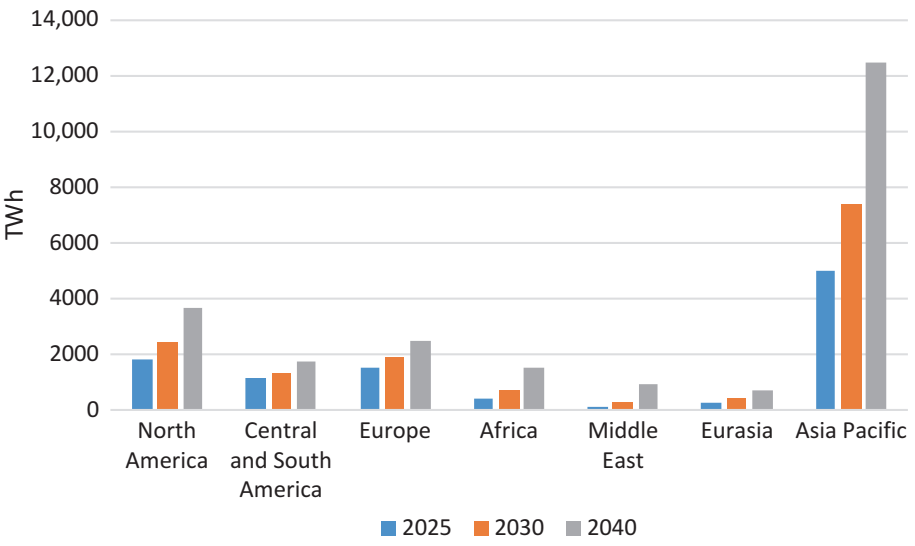

Fig. 8.9 Renewables demand under the IEA Sustainable Development Scenario, 2025–2040 (TWh). Source: IEA World Energy Outlook 2018

energy as a substitute for fossil fuels are its abundance and distribution; it is renewable, and has no greenhouse gas emissions. Although wind power is capital intensive and therefore requires upfront investment, it does not have any fuel costs, and therefore, like solar energy, has low-to-zero marginal costs.

The majority of installed wind power today are horizontal axis wind turbines (HAWT), with increases in average turbine capacity, rotor diameter and hub height the long-term trend. Wind turbines can be located either onshore or offshore, and currently reach up to 10 MW of onshore generation, and 12 MW for offshore generation. Offshore wind can be more consistent and have a higher velocity while having relatively higher construction and maintenance costs. One issue with wind energy is its consistency and variation over short time frames, and is therefore used in combination with other electricity generation assets and power management methods to meet demand schedules.

By the end of 2017, the total global installed wind turbine capacity was 539 GW, with an additional 52 GW of capacity added during the year, and total global wind turbine capacity able to meet greater than 5% of global electricity demand. Wind turbine energy capacity is widely distributed in Europe, with other regions increasingly migrating to wind energy power to meet global electricity demand.

Solar energy, or power from the sun, is a resource that is larger than every other energy source available on the planet, with approximately 174,000 terawatts (TW) of power provided constantly through solar radiation to the atmosphere's higher levels. Global power consumption was approximately 22,015 TWh as at 2017, and therefore, the solar energy that radiates to the planet is more than sufficient to supply total energy requirements. The solar resource is also freely accessible, and globally distributed relative to other energy resources.

Solar energy is a renewable energy that sources the Sun's radiant light and heat for a range of energy technologies that include photovoltaics, solar heat, solar thermal electricity and solar cells. These technologies can address energy security and climate change issues, and integrate into electricity systems. Solar energy is generally more available in countries with warm and sunny climates, which are also the regions that will see the majority of the global population and economic growth in the coming decades. The global population in warm and sunny climates is estimated to be 7 billion, compared to 2 billion in cold and temperate climates, by 2050.

Light, in general, concerns a particular type of electromagnetic radiation, that consists of oscillating electric and magnetic fields that vibrate at a given frequency and wave length, and disseminate linearly. The electricity produced by solar radiation to a semiconductor surface, directed at the sun on a clear

day at noon, is approximately one kilowatt per square meter. Silicon is a semiconductor solid comprised of electrons, a subatomic particle that has an electrical charge. A six-inch square silicon solar cell generates approximately 0.5–0.6 volts and 4–5 watts under direct sunlight with an intensity of one kilowatt per square meter. Solar cells are linked in a PV module in series to boost the combined output voltage. A PV module will typically be composed of 60–96 solar cells, and produce 30–48 volts and 260–320 watts of power. PV modules also include additional operational mechanical components, and are linked together as solar arrays, either in series to increase output voltage, or in parallel to increase output current.

Solar energy electricity technologies have the potential for large-scale growth, with global expansion reaching terawatt generation capacities. The recent rapid growth in solar generating capacity, technology, performance and price improvements, combined with innovative business model developments, have driven investment in commercial and residential solar systems. Two solar energy technologies that can scale for the generation of grid electricity are concentrated solar power (CSP) and photovoltaic (PV) systems.

Each technology has significant differences. CSP technologies offer large-scale installations, a generating capacity of 100 MW or greater and the ability to store thermal energy to generate electricity outside of periods with little or no sunlight. CSP systems use direct irradiance only, and are therefore more sensitive to the influence of cloud, haze and dust. CSP systems currently offer large-scale installations without the potential for materials availability bottlenecks, and the inclusion of thermal energy storage in CSP systems also provides a dispatchable electricity resource.

PV systems can use all solar radiation incident, and can be configured as utility plants that have greater than a 1 MW capacity, to residential installations under a capacity of 10 kW. The output of PV systems is sensitive to changes in solar radiation. PV costs by convention are split into solar module costs and balance-of-system (BOS) costs. BOS costs, or all PV system components other than the PV panels, include inverters, hardware, labour, financing, marketing and regulatory costs. Continuing developments in PV technology can also have an influence on solar module and BOS costs.

The competitiveness of solar energy in relation to other generation technologies is a function of the revenue and cost structures within a specific electricity market. Most installed solar electricity generation globally today is PV. There are three issues, however, that need to be addressed in regards to solar energy having a major role in the future energy mix. Although solar electricity costs have significantly declined in recent years, solar power is still

relatively more expensive than the current fossil fuel technologies in many regions, although this would be offset by carbon pricing. Currently, BOS costs account for approximately two-thirds of the price of utility-scale PV installations.

Second, the solar resource also fundamentally differs from other energy resources due to its intermittency at any location on the planet's surface. Predicting the solar resource is a function of both stochastic processes, with uncertainty occurring at frequencies that span minutes to days due to cloud cover and weather, and deterministic processes, with oscillations that have frequencies from days to months and are a function of the planet's daily rotations and seasons.

The third issue is scaling. Forecasting solar power at any location due to its intermittency can be a significant impediment to building large-scale solar generation in many regions. Matching generation with demand in electrical power systems is essentially a real-time process, with demand variations not entirely predictable. Solar generation within a power system will incrementally add volatility and reduce the net load predictability due to its intermittency.

The intermittency in renewable generation has been a key obstacle for contracts in the forward wholesale market, which are used to manage risk for generators and retailers in volatile electricity markets. Renewable generation is typically dispatched first as the electricity output cannot be regulated, has zero marginal generation costs and is paid the prevailing spot price. Solar firming contracts offer the ability to 'shape' contracts that match the load of buyers. A contract can replicate the shape of solar generation, for example, when there is no solar generation due to the time of day or the weather, and match a buyer's demand with supply contracts in the wholesale market, and therefore, provide a flat or fixed price. Developments in solar contracts include a solar shape and a solar firming, or inverse solar shape.

8.4 Energy Statistics

8.4.1 The Schwartz Single Factor Model

Energies such as electricity and natural gas exhibit the property of mean reversion. Modelling these price series using Black–Scholes-type models can produce unrealistic spreads between the two related energy commodities. Mean reversion can be captured in a more realistic single factor model introduced by

Schwartz (1997), which assumes that the spot price follows a mean reverting process:

$$dS = \alpha\left(\mu - \lambda - \ln S\right)Sdt + \sigma Sdz \tag{8.1}$$

where α is the mean reversion rate, which is the speed of adjustment of the spot price back towards its long-term level μ, σ is the spot price volatility and λ is the market price of energy risk. By defining $x = ln\ S$ and applying Itô's lemma to Eq. (8.1), the log price can be characterized by the Ornstein–Uhlenbeck process:

$$dx = \alpha\left(\hat{\mu} - x\right)dt + \sigma dz \tag{8.2}$$

where,

$$\hat{\mu} = \mu - \lambda - \frac{\sigma^2}{2\alpha}.$$

8.4.2 Schwartz Single Factor Futures and Forward Pricing

Futures and forward prices with maturity s in the Schwartz single factor model are equal with the appropriate boundary conditions and are given by:

$$F\left(t,s\right) = \exp\left[e^{-\alpha(s-t)}\ln S + \left(1 - e^{-\alpha(s-t)}\right)\left(\mu - \lambda - \frac{\sigma^2}{2\alpha}\right) + \frac{\sigma^2}{4\alpha}\left(1 - e^{-2\alpha(s-t)}\right)\right] \tag{8.3}$$

The mean reversion rate α determines how quickly forward prices revert to the long-term level. Figure 8.10 illustrates the sensitivity of the futures price defined in Eq. (8.3) to the mean reversion parameter, or the speed of mean reversion. The parameters used in the illustration are S = 110, σ = 0.3, λ = 0, μ = ln(100) and α = 0.1, 1 and 10. The long-term level of the futures curve does not equal exp(μ), as it is adjusted by an amount that depends on the relative size of α and σ:

$$F\left(t,\infty\right) = \exp\left[\mu - \lambda - \frac{\sigma^2}{4\alpha}\right] \tag{8.4}$$

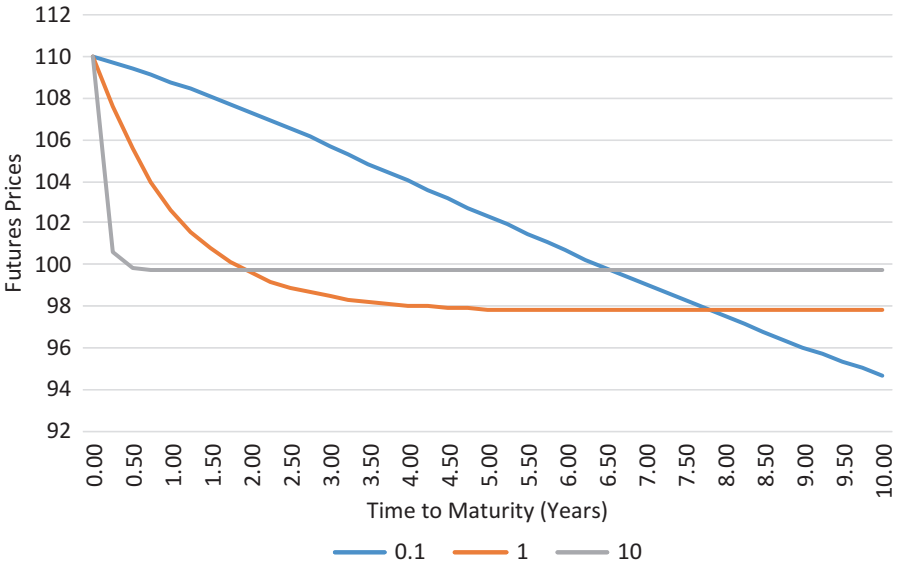

Fig. 8.10 Schwartz single factor model futures prices. Source: Clewlow and Strickland 2000

8.4.3 Volatility

The volatility measure used in energy pricing models should be estimated in the context of the specific stochastic price process that captures the key features of the energy markets, such as mean reversion. The constant volatility assumption used in the Black–Scholes model is not consistent with the empirical observation that long-dated energy forwards have less volatility than short-dated energy forwards.

Itô's lemma can be applied to Eq. (8.3) to provide the term structure of proportional futures volatilities in the single factor model:

$$\sigma_F(t,s) = \sigma e^{-\alpha(s-t)} \tag{8.5}$$

Figure 8.11 illustrates the effect of the speed of mean reversion, α in Eq. (8.5), on the term structure of volatility of futures prices. Volatility parameters of 0.3 and α = 0.1, 1 and 10 are used in the illustration. Increasing the speed of mean reversion, for example, increases the attenuation of the volatility curve. As the maturity of the forward increases, the volatility also tends to zero.

While the volatility term structure based on the Schwartz single factor model is a more accurate representation than the Black–Scholes model, its shape is still relatively simple. Even though a volatility function of this type

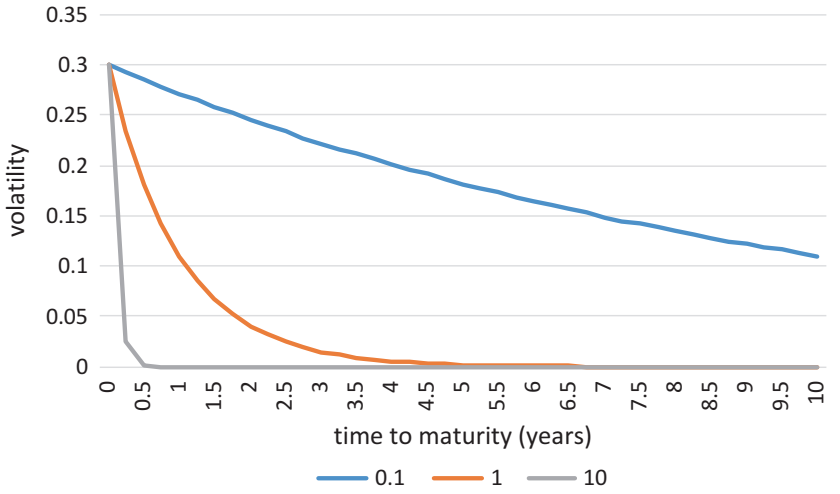

Fig. 8.11 Volatility of futures prices in the Schwartz single factor model. Source: Clewlow and Strickland 2000

describes the attenuation typical of market forward volatility term structures, the volatility parameters tend to zero for longer dated maturities. While market volatilities of forward energy prices do decrease as maturities increase, they typically do not approach zero, and therefore, the Schwartz model has a potential drawback when pricing options on long-dated maturity forward contracts.

This attribute obviously is not correct, and is a function of the simple assumptions in the form of mean reversion in Eqs. (8.2) and (8.5). This issue can be addressed in the representation of Eqs. (8.2) and (8.5) by directly specifying the volatility function, and adding a constant long-term level of forward price volatility to the simple negative exponential specification.

8.4.4 Correlation

The volatility of a spread is less than the sum of the volatilities of the individual components, and should be considered in the pricing of spread options. The correlation between two assets is captured by:

$$\xi_{1,t} = \varepsilon_{1,t} \tag{8.6}$$

$$\xi_{2,t} = \rho\varepsilon_{1,t} + \varepsilon_{2,t}\sqrt{1-\rho^2} \tag{8.7}$$

where $\xi_{1,t}$ and $\xi_{2,t}$ are two independent random numbers from a standard normal distribution, and ρ is the correlation between the two assets.

8.4.5 Simulating Mean Reversion

A Monte Carlo simulation simulates possible future values of an underlying asset using a stochastic process based on assumptions of the behaviour of the relevant market variables. The advantages of Monte Carlo simulation are that it can facilitate the accuracy in the modelling of market price behaviour by including factors such as jumps, seasonality, stochastic volatility and possible future structural changes in the market. The disadvantages are its relative complexity in implementation and the resources required for computation.

The mean reverting spot price model in Eq. (8.2) was specified in terms of the natural logarithm of the spot price $x = \ln(S)$:

$$dx = \left[\alpha\left(\mu - x\right) - \frac{1}{2}\sigma^2\right]dt + \sigma dz \tag{8.8}$$

which can be discretized as:

$$\Delta x_i = \left[\alpha\left(\mu - x_i\right) - \frac{1}{2}\sigma^2\right]\Delta t + \sigma\sqrt{\Delta t}\varepsilon_i \tag{8.9}$$

In contrast to the GBM (geometric Brownian motion) model, the discretization in this specification is only correct in the limit of the time step tending to zero, as the drift term is dependent on the variable x. Time steps that are relatively small to the speed of mean reversion should therefore be chosen. To simulate the path of the spot price, the parameters α, μ, σ and Δt are estimated, normally distributed random numbers ε_i are repeatedly generated and new values of Δx are calculated, from which a new spot price at each time step is then derived.

8.4.6 Estimating the Mean Reversion Rates

Two methods can be used to estimate the mean reversion rate α, either through linear regression using spot price data or by fitting the single factor volatility function to the empirical volatility term structure. The simple mean reverting process for the natural logarithm of the energy spot price:

$$dx = \alpha\left(\bar{x} - x\right)dt + \sigma dz \tag{8.10}$$

is essentially the same as Eq. (8.8), but with the $-½\sigma^2$ included in $\bar{x}$. This can be discretized as:

$$\Delta x_t = \alpha_0 - \alpha_1 x_t + \sigma\varepsilon_t \tag{8.11}$$

where $\alpha_0 = \alpha\bar{x}\Delta t$ and $\alpha_1 = \alpha\Delta t$. Observations of the spot price through time imply the linear relationship between Δx_t and x_t with the noise term $\sigma\varepsilon_t$. Regressing observations of Δx_t against x_t obtains $\alpha_0 = \alpha\bar{x}\Delta t$ and $\alpha_1 = \alpha\Delta t$ as estimates of the intercept and slope of this linear relationship. As the time interval between observations Δt is known, estimates of α and $\bar{x}$ can be obtained.

An alternative is to estimate α, the mean reversion rate, from the term structure of volatility. The volatility of short-term energy forward contracts is typically more volatile that long-term contracts, with the volatility declining as the maturity increases. Equation (8.12) represents this decline in the volatility as t gets large:

$$\sigma_1(t,T) = \sigma e^{-\alpha(T-t)} \tag{8.12}$$

where $n = 1$. The mean reversion rate of the spot energy price can be estimated through the relationship between the spot price process and single factor model described in Sect. 8.4.1.

8.4.7 The Jump Parameters

The combination of mean reversion and jumps into the same model can be represented by the stochastic differential equation (SDE):

$$dS = \alpha(\mu - \ln S)Sdt + \sigma Sdz + \kappa Sdq \tag{8.13}$$

The mean reversion jump-diffusion model can be discretized as:

$$\Delta x_t = \left[\alpha(\mu - x_t) - \frac{\sigma^2}{2}\right]\Delta t + \sigma\sqrt{\Delta t}\varepsilon_{1i} + (\bar{\kappa} + \gamma\varepsilon_{2i})(u_i < \phi\Delta t) \tag{8.14}$$

where u_i is a uniform (0,1) random sample, and ε_{1i} and ε_{2i} are independent standard normal random variables. The term $(u_i < \phi\Delta t)$ returns one if true and zero if false, and generates the random jumps with the average frequency.

The jump size when it occurs is the mean jump size, represented by $\bar{\kappa}$, plus the jump standard deviation γ scaled by ε_2 to derive a normally distributed random shock. The time step Δt should be small in relation to the jump frequency, where $\phi \Delta t << 1$, so that the simulation of the jump frequency is accurate. dS is sum of the GBM mean reversion process and $\left(\bar{\kappa} + \gamma \varepsilon_{2i}\right)$ if a jump occurs. The Weiner and Poisson processes are assumed to be independent and not correlated, and therefore, the jump process is independent of the mean reversion process.

Estimating energy price jump parameters is complex in that the observed jumps are a subset of the time series, which also includes the non-jump price behaviour. The exact arrival of a jump is unknown, and the probability of these large price spikes within a GBM is effectively zero. The following jump parameters can be estimated using the recursive filter method:

ϕ = number of jump returns divided by the number of jumps within the sample
$\bar{\kappa}$ = average jump size of returns
Γ = standard deviation of jump returns

The standard deviation of the price returns is used to derive a probability for the identification of outliers that are greater than the chosen probability for actual jumps. The diffusion volatility is then re-estimated by deriving the standard deviation of the price returns with the jumps removed. The new diffusion volatility is then used to identify those jumps that exceed the probability limit, with the process repeated to where the estimates converge and no new jumps are identified.

8.4.8 The Half-Life of a Mean Reverting Process

A key property of a mean reverting process is the half-life. This is the time taken for the price to revert half-way back to its long-term level from its current level if no more random shocks arrive. Ignoring the randomness allows a focus on the mean reverting behaviour itself. The half-life, denoted by $t_{1/2}$, can be derived as:

$$t_{1/2} = \ln(2) / \alpha \tag{8.15}$$

The half-life is an average over a long time period, representing the time that shocks to the spot price take to decay to half their deviation from the

long-term level. Table 8.1 illustrates the range of half-lives for various values of alpha.

8.4.9 Energy Spot Price Model Simulation

Figure 8.12 illustrates a simulation using Eq. 8.14 of a mean reversion jump diffusion path for an electricity spot price, where $\overline{S}$ is the long run mean, ϕ is the average number of jumps per dt, $\overline{\kappa}$ the average jump size of returns is set to zero, and γ is the standard deviation of jump returns. The function $\left(u_i < \phi\Delta t\right)$ takes a value of one if true and zero otherwise, and generates jumps at a random frequency as defined by ϕdt. If a random number is generated below the average jump frequency, a jump is simulated in a random direction, while if above the frequency, then no jump is generated. The jump size when

Table 8.1 Mean reversion rates and the corresponding half-lives

α	$t_{1/2}$
1	8 months
10	25 days
100	2.53 days
1000	6 hours

Source: Clewlow and Strickland (2000)

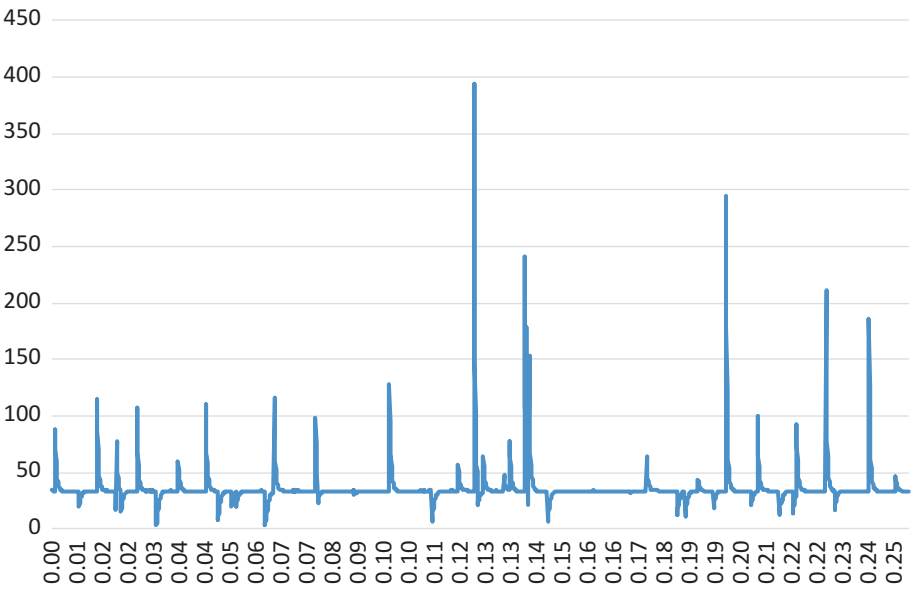

Fig. 8.12 A mean reversion jump diffusion electricity spot price simulation

it occurs is the average of the historical jump returns plus the jump standard deviation γ multiplied by a uniform normally distributed random variable, with the probability of either positive and negative jumps occurring. As the mean jump size is typically problematic in the derivation of robust estimates, it is set to zero. The half-life is 3 hours, which is derived as $\ln(2)/2000 \times 24 \times 365$.

$$\text{Price} = 35,\ \alpha = 2000,\ \bar{S} = 35, \sigma = 30\%,\ \bar{\kappa} = 0,\ \phi = 250,\ \gamma = 1.2,\ \Delta t = 1/(24 * 365)$$

The single factor model is a relatively simple model for the forward curve. While the volatility structure under the Schwartz single factor model is more realistic than the Black–Scholes model, it still has a relatively simple shape, and the volatilities tend to zero for longer maturities. The single factor model in Sect. 8.4.1 can be generalized and modified, as illustrated in Sect. 6.4, to include multiple sources of uncertainty in the forward curves. Clewlow and Strickland (2000) value energy options in a general multi-factor model for the forward curve, which can capture multiple sources of uncertainty. As spread options depend simultaneously on forwards related to separate energies, Clewlow and Strickland extend the multi-factor model to a specification that can simultaneously model a number of different energy forward curves, and capture the multiple dynamics of the forward curves in the valuation of spread options.

8.4.10 Wind Power Statistics

The conventional methodology for utilizing wind resources for the generation of electricity is the use of power curves. Wind turbine power curves provide values for the production of electricity as a function of wind speed at the turbine hub height and turbine type. Wind is measured in metres per second (m/s), with 10 (m/s) an established measure. A wind power curve is described by variables on two axes, v(m/s), the hub height wind speed on the horizontal axis, and power (MW) on the vertical axis, and has three significant values on the wind speed axis:

- The cut-in speed—the minimum wind speed at which the turbine delivers power.
- The rated output speed—the initial point on the wind speed axis at which the maximum turbine rated power is generated.
- The cut-out speed—the maximum wind speed for the turbine power generation, above which generation is zero.

Table 8.2 Typical features of a power curve

Characteristic	Value (m/s)	Power output (MW)
Cut-in wind speed	3	P_{min} = 0.0533
Rated wind speed	11.5	P_{rated} = 4.5
Cut-out wind speed	25	–

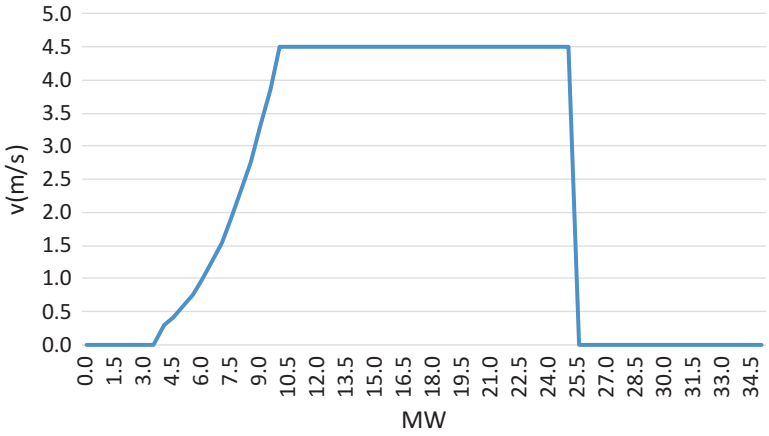

Fig. 8.13 The assumed wind turbine power curve

Table 8.2 illustrates the three significant values for a power curve example with a hub height of 100 m and a rated power of 4.5 MW.

While wind turbine model types have unique power curves that are specific to the manufacturer, the power curve in Fig. 8.13 is a common representation based on the data in Table 8.2.

The power obtained from wind is described by a cubic function:

$$P_{wind}(v) = \left(\frac{1}{2}\right) pA^3 \tag{8.16}$$

where,

$P_{wind}(v)$ = power (Watts)
P = 1.225 kg/m^3 (air density)
A = the rotor swept area (m^2)
v = hub height wind speed (m/s)

The rotor swept area is derived as:

$$A = \pi \left(\frac{rotor\ diameter(m)}{2} \right)^2 \tag{8.17}$$

For example, for a 100 m rotor diameter, the swept area is 7854 m^2. Annual potential wind energy is calculated as wind power (kW) multiplied by 365 × 24.

The power generated by the wind turbine between the cut-in speed and the rated speed is scaled by an efficiency parameter C_p:

$$P_{turbine}(v) = \left(\frac{1}{2} \right) pAC_p v^3 \tag{8.18}$$

The power coefficient *Cp* is the Betz limit, or the maximum power that can be generated from wind at the site, and is the ratio of 16/27 or 59%, the Betz coefficient. The potential maximum wind power in Watts is therefore:

$$59\% * P_{wind}(v). \tag{8.19}$$

A power curve is, therefore, described by the following, with $P(v)$, the power output, a function of v, the hub height wind speed (m/s):

0, where $v \leq v_{cut\text{-}in\ speed}$

$\left(\frac{1}{2} \right) pAC_p v^3$, where $v_{cut\text{-}in\ speed} < v \leq v_{rated\ power}$

$P_{rated\ power}$, where $v_{rated\ power} < v \leq v_{cut\text{-}out\ speed}$

0, where $v_{cut\text{-}out\ speed} \leq v$

The Weibull probability distribution is typically used to describe a wind turbine power output, and is characterized by two parameters for 10-minute average wind speeds—v, the hub height wind speed (m/s), and c, a scale parameter. A value of 2 for the Weibull shape parameter, k, is consistent with annual wind speed distributions. The parameter c can therefore be derived for an assumed wind speed:

$$c = \frac{\overline{v}}{\Gamma(1 + 1/k)} \tag{8.20}$$

where,

$\overline{v}$ = the average wind speed for $1 \leq k < 10$
$\Gamma(x)$ = the gamma function.

For an average wind speed of 10 (m/s), c is equal to 11.28. The Weibull probability density function is therefore:

$$f(v) = \frac{k}{c}\left(\frac{v}{c}\right)^{k-1} e^{-(v/c)^k} \text{ for } v \geq 0 \tag{8.21}$$

and 0 for $v < 0$.

The shape of the Weibull distribution is a function of the turbine location and time frequency, with the parameters k and c estimated and fitted according to the wind turbine location. Figure 8.14 illustrates the Weibull distribution that describes the yearly wind speed for $k = 2$ and $c = 11.28$.

The shape parameter k can also be estimated based on the assumptions in regards to the average wind speed and the wind volatility:

$$k = \left(\frac{\sigma_v}{\overline{v}}\right)^{-1.086} \tag{8.22}$$

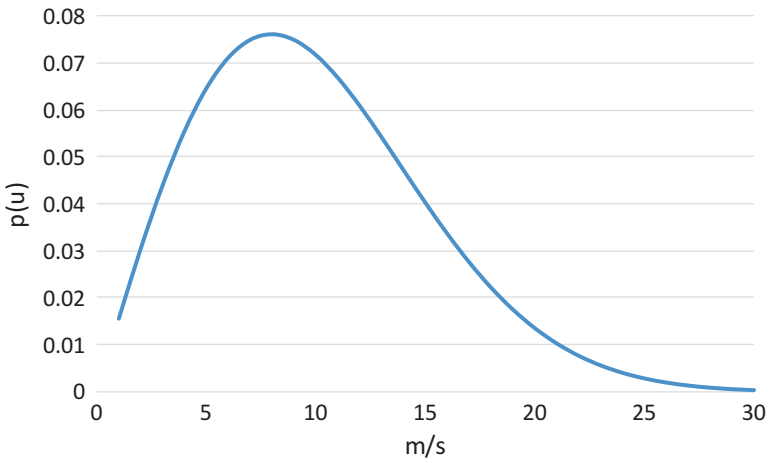

Fig. 8.14 Weibull distribution for $k = 2$, $c = 11.28$

where $\overline{v}$ is the average wind speed, and σ_v is the standard deviation of wind speed, derived as:

$$\sigma_v = \overline{v}^2 \left[\frac{\Gamma\left(1+2/k\right)}{\Gamma^2\left(1+2/k\right)} - 1 \right] \tag{8.23}$$

The empirical relationship between the three parameters, k, c and $\overline{v}$ is specified as:

$$\frac{c}{\overline{v}} = \left(0.568 + \frac{0.433}{k} \right)^{-1/k} \tag{8.24}$$

Using the underlying assumptions in regards to the wind turbine power curve and the wind speed probability distribution, a wind farm capacity factor can then be derived. The capacity factor is the ratio of:

$$Capacity\ factor = \frac{average\ annual\ production\ MWh}{nameplate\ capacity\ (MW) \times 365\ days \times 24\ hrs} \tag{8.25}$$

where the nameplate capacity is the wind turbine maximum output rating. The average power generated $E[P(v)]$ is the power curve multiplied by the Weibull probability distribution:

$$E\left[P\left(v\right)\right] = \int_{v_{\min}}^{v_{\max}} P\left(v\right) f\left(v\right) dv \tag{8.26}$$

An additional parameter is required for the wake effects produced by a wind turbine within a wind farm. The clustering of wind turbines can reduce the total energy converted to electricity relative to the energy generated by the individual turbines operating under the same wind flow conditions. A turbine's downwind wind speed is inevitably less than its upwind wind speed, and therefore, upstream turbines 'shadow' downwind turbines. The downwind and cross spacing of wind turbines at the site can, however, maintain losses from wake effects at less than 10% of the wind farm power generation.

Table 8.3 summarizes the variables and parameters for a wind turbine and wind farm.

Table 8.3 Summary of the variables and parameters

Wind resource		Wind turbine		Wind farm	
v	10 m/s	Rated power	4.5 MW	Loss factor	10%
Shape factor	2	Cut-in speed	3 m/s		
Scale factor	11.28	Rated speed	11.5 m/s		
		Cut-out speed	25 m/s		
		Cp	59%		

8.5 Natural Gas Generation Valuation

8.5.1 Overview

Natural gas (NG) is a fossil fuel in which the principal element, methane, is a hydrocarbon, a compound that consists of hydrogen and carbon. Technologies for the generation of electricity through the combustion of natural gas include simple cycle turbines, conventional steam and combined cycle gas turbines (CCGT). Simple cycle combustion turbines are typically used for peak electricity demand, while conventional steam electricity turbines account for the majority of electricity generation. A CCGT plant combines a gas and steam turbine to generate electricity, and can produce significantly more power than simple cycle plants from the equivalent fuel. The growth in renewable capacity has increased the intermittency in the electricity supply, creating a structural change in the generation load and the need for increased flexibility in the power system. CCGT generation assets, by design, are well suited to respond to this requirement with their ability to ramp up within minutes and meet peak or unscheduled demand loads. Natural gas power generation generally produces relatively less emissions that other fossil fuels such as oil and coal, and is considered a bridge fuel as the energy mix transitions to clean energy.

The valuation of power plants is typically conducted for M&A (mergers and acquisitions) transactions, business entity going concerns and value analysis, and by convention, uses the intrinsic value, where value is a function of the plant dispatch relative to electricity prices in the forward market. The dispatch model values plants by determining the marginal cost-based clearing price and calculating cash flows based on the intrinsic spread, the spark spread, between the electricity price and the cost of fuel for generation. The margin received, or the spark spread, is derived over the life of the plant and discounted to the present.

The problem with the industry standard dispatch model is that it takes no account of volatility. Although the intrinsic discounted cash flow (DCF) model recognizes that a peaking plant has intrinsic value, that is, electricity

prices can increase to a point where there is value in switching on the plant, it does not capture value derived from the volatility in the spark spread. The extrinsic value method is therefore increasingly being used in valuation, as flexibility now has a significant role in the use of NG power generation assets. Although CCGT generators are able to hedge some of the intrinsic value during peak loads, a greater percentage of the asset value is extrinsic.

A power plant's extrinsic value can account for the value derived from the volatility within the electricity and NG spark spread, and valued as a portfolio of European electricity and NG spread options. Power peaking plants valued as options on the fuel cost and power price spread provides the owner, or option holder, with the right to operate the unit when electricity prices are higher than the cost of the fuel used to generate. A portfolio of peaking units can increase marginal value significantly.

The operating characteristics of a NG power generation plant can therefore be defined as the equivalent to a spark spread option. A peaking plant can choose to only run when the power price exceeds the marginal fuel cost. The real option in the peaking plant is the ability to choose whether to generate or not at a given power price. While the peaking plant may have available capacity, there is no obligation to generate, regardless of the electricity price.

A rational generator operator would choose to generate when power prices are above the fuel cost and any start-up costs. These real options are switching options, defined in the following valuation example as a series of European call options on the spark spread between power and NG prices. Valuing the power plant as a real option illustrates the value in the flexibility to call the plant when the energy spread is positive, which can be used to optimize operations—and therefore, value.

8.5.2 Energy Forward Curves

Capturing the significant features of the energy markets is important in applications of energy pricing models. Although a number of energy derivative models use forward curves for pricing, there are some associated problems. Energy forward curves are typically composed of discrete monthly futures contracts, and therefore, are not continuous as assumed in the pricing model. Some energy markets can be in *backwardation* (where futures prices are lower than spot prices) while others might be in *contango* (where futures prices are higher than spot prices), which gives the spread its own forward curve. The spread can also become negative as a consequence of these properties. Another issue is that seasonality can also exist in the spreads.

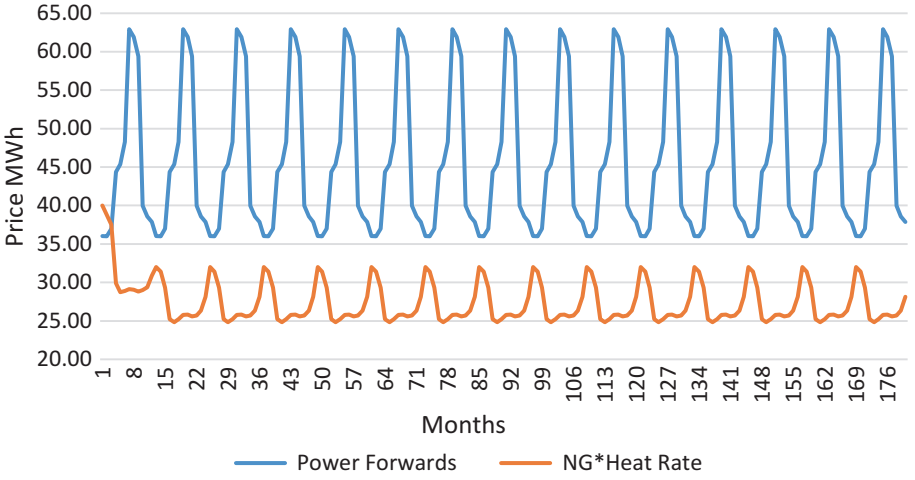

Fig. 8.15 The spark spread forward curves

Figure 8.15 illustrates the forward curves used in the valuation example. The forward curves were derived for the following valuation example, with annual seasonal patterns and negative spark spreads from January to March for each year.

Although electricity cannot be easily stored, the fuels used to generate the electricity can be stored, and the link between the two implies that the forward curve for electricity should be related to the input fuels. An arbitrage pricing approach takes this into account by considering the conversion process.

One of the key steps in the conversion process is the generation process itself, and this depends on the efficiency of generation expressed as the heat rate, the number of British Thermal Units (Btu) required to generate one kWh of electricity. A basic electricity forward curve can be obtained for the fuel forward curve via the following relationship:

$$Cost_{electricity} = Heat\ Rate \times Price_{fuel} \tag{8.27}$$

A constant value of the heat rate implies that the shape of the electricity forward curve should resemble the forward curve of the input fuel. The cost of electricity can be converted into a forward price after taking into account costs associated with fixed assets, transmission and tolling charges and others, such as fuel storage and fuel transportation. These costs obviously change through time.

Forward energy curves can be created as composite curves that consist of market data such as futures, forward prices and curve modelling. One feature exhibited by energy prices is the high level of seasonality, a repetitive cyclical pattern in the price over time. Seasonality in the power markets is driven typically by demand caused by weather factors such as hot summer months.

8.5.3 Energy Derivatives

There are a number of practical problems associated with derivative modelling in energy markets. Some of the important issues associated with energy derivative pricing that were often overlooked in early modelling approaches are:

- Energy prices tend to be drawn to production costs. The geometric Brownian motion (GBM) assumption permits price series to drift to unrealistic levels when applied to energy markets. In the short run, divergence from the cost of production can be possible under abnormal market conditions; however, in the long run, supply will adjust to the anomaly and prices will move to the level determined by the cost of production. This property is described as mean reversion.
- Energy prices display seasonality. Seasonality in energy prices and volatility may correspond to the time of year, such as winter or summer, and also can result from regular demand patterns due to factors such as the weather.
- Energy commodities cannot be treated solely as financial assets, as energy commodities are inputs to production processes and/or consumption goods. Models based on an automatic extension of those developed for financial markets may therefore break down when applied to energy markets.
- Another problem with applying the GBM assumption to energy prices is that their market price behaviour is often not consistent with the assumption of price continuity over time. Commodity and energy prices often display jump behaviour, determined in many cases by fluctuations in demand and supply. The frequency of these extreme values is often larger than the probability implied by GBM models.

In some markets, such as energy, the concept of being able to perfectly replicate options by continuously trading the underlying asset can be unrealistic. Many energy derivatives, however, actually rely on futures prices rather than the spot price, with the prompt futures contract a proxy for the spot price, and therefore, futures can be used to replicate options positions and permit the application of the risk-neutral pricing approach.

8.5.4 Energy Spread Options

The payoff in a spread option is derived from the price differential between two underlying assets. These types of exotic options can be used either to take a position on, or to hedge the risk associated with, the relative performance of two underlying assets. The payoff of a European spread call option at maturity T is:

$$c = \max\left[S_{1T} - S_{2T} - K, 0\right] \tag{8.28}$$

where S_{1T} and S_{2T} are the spot prices of the two underlying assets, and K is the exercise price.

Most option pricing models have the underlying assumption that the risk-neutral price distribution of the underlying asset is lognormal. A spread option is priced as the discounted double integral of the option payoffs over the risk-neutral distribution of the two underlying assets at maturity T (Pearson, 1997).

Analytical Black–Scholes-type models for valuing spread call and put options that include a strike are not known, and therefore, the Kirk approximation method is used in the following valuation illustration.

The Kirk approximation formula for the pricing of European call spread options on futures or forwards is:

$$C \approx \left(F_2 + K\right)\mathrm{e}^{-r(T-t)}\left(FN\left(d_1\right) - N\left(d_2\right)\right) \tag{8.29}$$

which can be rewritten as:

$$C \approx \mathrm{e}^{-r(T-t)}\left(F_1 N\left(d_1\right) - \left(F_2 + K\right)\right)N\left(d_2\right) \tag{8.30}$$

where,

$$\sigma \approx \sqrt{\sigma_1^2 + \left(\sigma_2^2 \frac{F_2}{\left(F_2 + K\right)}\right)^2 + 2\rho\sigma_1\sigma_2\left(\frac{F_2}{\left(F_2 + K\right)}\right)}$$

$$F = \frac{F_1}{\left(F_2 + K\right)}$$

$$d_1 = \frac{\ln\left(F\right) + \left(\frac{\sigma^2}{2}\right)\left(T-t\right)}{\sigma\sqrt{T-t}}$$

$$d_2 = d_1 - \sigma\sqrt{T-t}$$

and F_1 is the power forward price, F_2 is the natural gas forward price times the heat rate, and K is the strike.

If the futures contracts underlying the option are written on two separate energies—in this case, natural gas and electricity—then the option is referred to as a *spark spread option.* Firms exposed to the price differences between two different energies often use options of this type. In this case of a natural gas-fired power generator, energy is an input into a process that produces another type of energy. If $F_a(t,T)$ represents the price of a T maturity futures contract on energy a—in this case, power—$F_b(t,T)$ represents the price of a T maturity futures or forward contract on energy b—in this case, NG times the heat rate—and K represents the start-up costs, then the payoff for a European call option with maturity T and strike K on the spread between the two forward contracts is:

$$c = Max\left(F_a\left(t,T\right) - F_b\left(t,T\right) - K, 0\right) \tag{8.31}$$

and therefore, the value of the call option at time t can be written generally as:

$$= P\left(t,T\right)\mathrm{E}_t\left[Max\left(F_a\left(t,T\right) - F_b\left(t,T\right) - K, 0\right)\right] \tag{8.32}$$

where $P(t,T)$ is the continuously compounded discount factor.

8.5.5 Natural Gas Peaking Power Plant Valuation

The assumptions for the valuation analysis are:

- The plant output is 300 MWh.
- The heat rate is 10,000—to derive the spark spread, the heat rate is divided by 1000.
- The generation plant has a total remaining life of 15 years.

- The power and natural gas forward curves consist of a series of one-month forward prices that represent the hourly average over each month.
- The plant will run 16 hours per weekday, except in the summer months of July, August and September, when it will run 24-hours per weekday.
- The start-up cost is $5000 per start-up.
- The MWh start-up cost was derived per month as the number of start-ups per month times $5000, which is divided by the total operating hours per month times the number of MWs.
- The operations and maintenance (O&M) costs are $1.50 per MWh.
- The discount rate is 6.50%, with the maturity for each discount factor the middle of each month.
- The power and natural gas monthly volatility curves represent the average volatility of the hourly average forwards for each month.
- The middle of each month is used as the maturity or expiry date for each spread option.
- The strike K represents the start-up costs, which is reflected in the per MWh start-up costs for each month.
- The 10% correlation (rho) between the two assets was estimated from spot price returns. Although there is typically a term structure of correlation similar to the term structures for forward prices and volatility, the correlation (or rho) between the volatilities is defined as a constant term in the valuation example.

Figure 8.16 illustrates the power and natural gas volatility term structure.

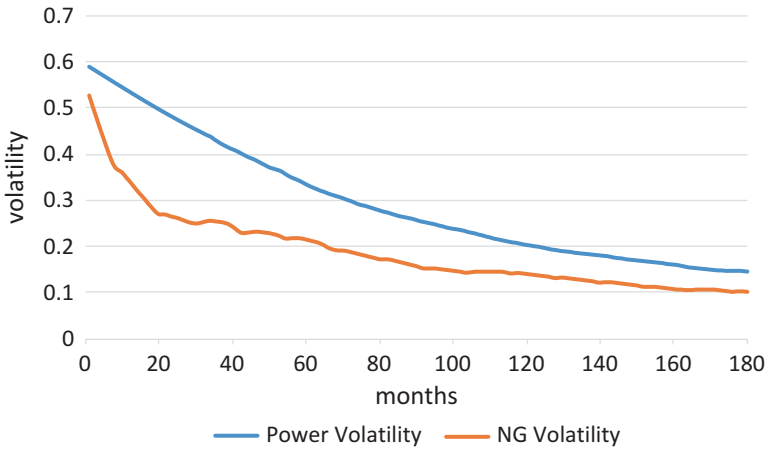

Fig. 8.16 The power and natural gas volatility curves

8.5.6 Energy Analysis and Valuation

Table 8.4 illustrates the intrinsic and extrinsic valuation of the natural gas peaking power plant. The intrinsic net present value (NPV) of the power plant is the sum of the present values of the net cash flows for each month. The spark spread options are priced as a series of European call spread options, with payoffs as specified in Eq. 8.32 from t_0 to T_i, the maturity or expiry for each European call spread option (in this case, the middle of each month) for each of the 180 European spread options. The extrinsic value equals the sum of spark spread options for each maturity. The intrinsic DCF valuation is $236.6 M while the spread option valuation is $301.8 M. While the DCF method does capture the intrinsic value, it does not account for the value in the volatility in the spark spread.

Figure 8.17 compares the spread option values and the DCF intrinsic values by month. The peaking plant is essentially an out-of-the-money option for at least part of the year. Although the spark spread can be negative, as is the case from January to March, the relatively large volatility associated with

Table 8.4 NG power generation intrinsic and extrinsic valuation

Month	1	2	3	4	....	179	180
Power forwards	36.02	36.00	37.00	44.36	....	38.57	37.88
Gas forwards	4.00	3.88	3.75	2.99	....	2.63	2.81
NG∗heat rate	40.00	38.80	37.50	29.90	....	26.32	28.12
Spark spread – $/MWh	−3.98	−2.8	−0.5	14.46	....	12.25	9.76
Start-up costs	0	0	0	14.46	....	12.25	9.76
Total operating hours	384	384	384	384	....	384	384
Total revenue $	0	0	0	1,545,792	....	1,291,200	1,004,352
Total O&M costs $	172,800	172,800	172,800	172,800	....	172,800	172,800
Net cash flows $	(172,800)	(172,800)	(172,800)	1,372,992	....	1,118,400	831,552
Discount factor	0.9963	0.9927	0.9891	0.9854	....	0.5186	0.5167
NPV $	(172,167)	(171,537)	(170,909)	1,352,994	....	580,024	429,680
Time to maturity (T)	0.08	0.17	0.25	0.33	....	14.92	15.00
Strike (K)	1.04	1.04	1.04	1.04	....	1.04	1.04
Power σ	59.1%	58.6%	58.1%	57.6%	....	14.8%	14.7%
NG σ	52.8%	50.3%	47.9%	45.5%	....	10.1%	10.0%
Net option value[a]	(14,923)	148,385	349,212	1,516,525	....	799,240	704,388
Kirk unit price	1.36	2.78	4.51	14.64	....	7.72	6.89
σ	74.37%	72.51%	70.74%	68.86%	....	16.83%	16.73%
F	0.8776	0.9036	0.9600	1.4337	....	1.4096	1.2990
$d1$	−0.5006	−0.1945	0.0614	1.1048	....	0.8532	0.7277
$d2$	−0.7153	−0.4905	−0.2923	0.7073	....	0.2031	0.0797

[a]Note: Option value net of total O&M costs

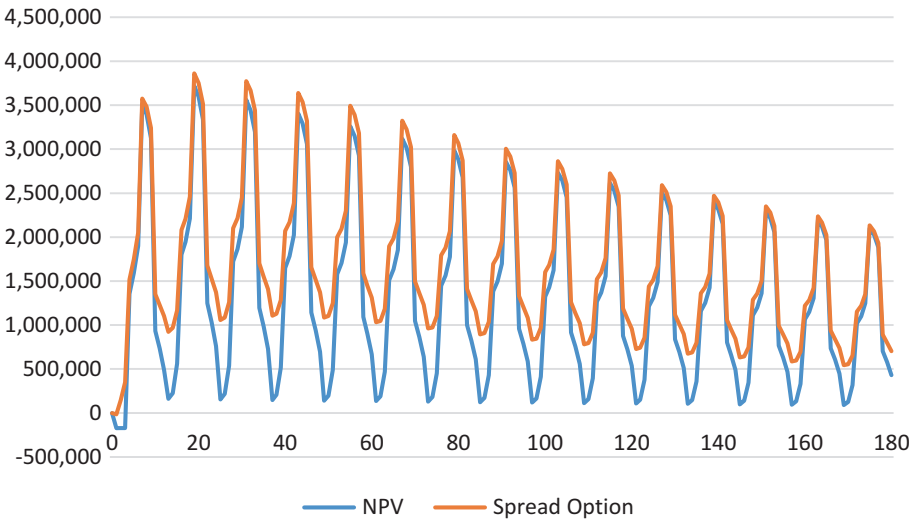

Fig. 8.17 Spread option and DCF intrinsic values by month

the energy markets implies that there is time value in the option, as there is some probability that the spark spread can be positive in these months. Consequently, the intrinsic DCF valuation of the peaking plant is likely to understate the value of the NG power generation plant. Value can also be maximized by considering the natural gas power generator as an asset that can be traded through its option value.

A number of factors can have an influence on the value of natural gas power generator. The 15-year life used for the power plant in this case study is arbitrary, and can feasibly be extended to value a new power plant. A benchmark for the cost of building a natural gas power plant is US$500,000 per MW. For the 300 MW NG generator illustrated in this case study, therefore, the cost to build would be US$150,000,000 million.

The value captured by including the volatility in the valuation will therefore have a significant impact on management decisions such as whether to build, divest or shut down a generator. Another driver of value that will influence decisions is the heat rate, the efficiency at which natural gas is converted into electricity. New natural gas generators will typically have lower heat rates than older plants, which will produce a relatively wider spark spread, and therefore have a competitive advantage over older generators.

Bibliography

BP Energy Outlook 2018.
Challa, R. Discovering multiple interacting options, Energy and Power Risk Management, July 2000.
Chignell, S, Robert Gross, R. Not locked-in? The overlooked impact of new gas-fired generation investment on long-term decarbonisation – A case study of lock-in to new CCGT in the UK, Imperial College Centre for Energy Policy and Technology Working Paper Ref: ICEPT/WP/2010/012, May 2012.
Clancy, H. Microsoft has figured out a way to reduce risks associated with PPAs, Greenbiz.com, October 16 2018.
Clewlow, L. and Strickland, C. Energy Derivatives, Pricing and Risk Management, Lacima, 2000.
Clewlow, L. and Strickland, C. Implementing Derivative Models, Wiley, 1998.
Financial Times. Sheppard D, Raval, A. Oil producers face their life or death question, June 19 2018.
Financial Times. Sheppard, D. Peak Oil forecast for 2036, July 2018.
Fortune. Ball, J. Shell Faces Lower Forever, February 1 2018.
IEA Key World Energy Statistics 2018.
IEA New Policies/Sustainable Policies.
IEA World Energy Outlook 2018.
Johnson, K, Thomas, N. Wind farm control addressing the aerodynamic interaction among wind turbines, 2009 American Control Conference, St Louis, Missouri, 2009.
Kirk, E, Correlation in the energy markets, Managing Energy Price Risk, Risk Publications (1995).
MIT Energy Initiative. The future of solar energy, 2015.
Parkinson, G. New solar "firming" contracts to boost corporate demand for big solar farms. reneweconomy.com, April 23 2018.
Schwartz, E.S. The stochastic behaviour of commodity price: implications for valuation and hedging, The Journal of Finance, LII(3): 923–73, 1997.
Shell energy transition report 2018.
U.S. Energy Information Administration Outlook 2017.
Wind Energy Explained: Theory, Design and Application, J F Manwell, J G McGowan and A L Rogers, 2nd edition, John Wiley and Sons, 2009.
World Wind Energy Report 2019.